buildings

Article

Web Crippling Behaviour of High-Strength Aluminium Alloy Channel Sections under Concentrated Loading: Numerical Modelling and Proposed Design Rules

Gang Sun, Xiao-Yong Sun * and Jian-Hang Fu

Department of Civil Engineering, Hebei University of Water Resources and Electric Engineering, Cangzhou 061001, China; sungang@hbwe.edu.cn (G.S.); 13171983102@163.com (J.-H.F.)
* Correspondence: 18045624023@163.com

Abstract: Two types of high-strength aluminium alloy (HA)—namely, AA-6086 and 7075-T6—have been developed and extensively used in recent years. These high-strength aluminium alloys offer advantages such as lower prices and higher yield strength than traditional alloys. The webs of aluminium channel members under concentrated loads are susceptible to web buckling failure, which restricts their applications. However, no research work has been reported that has evaluated the web buckling performance of high-strength aluminium alloy channel sections subjected to end-two-flange (ETF) loading, and the material characteristics of these high-strength aluminium alloys differ significantly from those of conventional aluminium alloys. This work addresses this gap by conducting a detailed numerical investigation. A parametric investigation consisting of 1024 models was performed using the finite element (FE) models previously developed for traditional aluminium alloys. A wide range of high-strength aluminium alloy sections covering varying web slenderness ratios, internal corner radii, bearing lengths, and aluminium alloy grades were considered in this investigation. It was shown that the latest design recommendations in the Australian and New Zealand Standards (AS/NZ S4600) and (AS/NZS 1664.1) were over-conservative when estimating the web buckling strength of such channel sections. Finally, new web buckling design equations for high-strength aluminium alloy channel sections were proposed through reliability analysis in this investigation.

Keywords: high-strength aluminium alloy; web buckling; end-two-flange loading; numerical modelling; proposed design rules

Citation: Sun, G.; Sun, X.-Y.; Fu, J.-H. Web Crippling Behaviour of High-Strength Aluminium Alloy Channel Sections under Concentrated Loading: Numerical Modelling and Proposed Design Rules. *Buildings* **2023**, *13*, 1823. https://doi.org/10.3390/buildings13071823

Academic Editor: André Rafael Dias Martins

Received: 7 June 2023
Revised: 5 July 2023
Accepted: 11 July 2023
Published: 19 July 2023

1. Introduction

Aluminum alloys are being increasingly used as building materials in structural engineering applications because of their numerous benefits, including being lightweight, highly resistant to deterioration, and easy to manufacture—as illustrated in Figure 1. In recent times, two types of channel sections fabricated by extrusion using high-strength aluminum alloys (HAs) AA-6086 and 7075-T6 have been extensively used due to their lower cost and higher yield strength [1,2]. However, the webs of aluminum channel members are prone to web buckling when subjected to concentrated loading, as aluminum alloys have a lower elastic modulus than steel. Therefore, the impact of web buckling on the performance of HA channel sections should be evaluated carefully.

The use of aluminum alloy sections as load-bearing members subjected to different loadings has been investigated by many researchers [3,4]. Roy et al. [5,6] and Fang et al. [7,8] numerically and experimentally studied the buckling performance and design of a back-to-back built-up aluminum alloy channel section subjected to axial compression, and the impacts of modified slenderness, screw number, and section thickness were evaluated. Feng et al. [9] reported the results of twelve laboratory tests on the flexural capacity of perforated aluminum members subjected to bending, and they found that the current design guidelines are normally over-conservative when estimating the flexural capacity of such channel sections.

Figure 1. Aluminum alloy sections used as load-bearing members in engineering applications.

Researchers have carried out a significant number of studies to evaluate the web buckling performance of cold-formed steel (CFS) sections over the last few years. Examples include Uzzaman et al. [10,11], Janarthanan et al. [12,13], Chen et al. [14], and Gunalan and Mahendran [15]. Web buckling failure in CFS beams was first experimentally investigated by Winter and Pian [16], and they reported a total of 136 laboratory test results. Following this, Young and Hancock [17] carried out web buckling laboratory testing on CFS beams featuring both restrained and unrestrained flanges. Macdonald et al. [18,19] observed that the web's bearing length, corner radius, and clear height significantly affected the member's web buckling strength. The web buckling performance of CFS hollow flange channel beams under two-flange loading was evaluated by Keerthan and Mahendran [20]. Using both laboratory testing and numerical methods, Sundararajah et al. [21,22] developed new design rules in web buckling strength using the Direct Strength Method (DSM).

Limited research works are available regarding the web buckling performance of aluminum channels. Alsanat et al. [13–27] recently evaluated the web buckling failure of aluminum sections with fastened flanges experimentally and numerically; they thoroughly assessed the existing design guidelines and suggested new ones based on their evaluation results. Zhou and Young [28] experimentally evaluated the web buckling performance of aluminum alloy channels, with 340 data points reported. They found that the latest design recommendations were generally unconservative and unreliable for those members with one flange-restrained condition.

However, all of the studies mentioned above were mainly focused on traditional aluminum alloy sections or CFS sections [29], despite the popularity of HA channels. No research study has been reported investigating the web buckling strength of HA channels subjected to end-two-flange (ETF) loading. In a recent study, Alsanat et al. [23] evaluated the web buckling performance of traditional aluminum alloy channels and presented new design recommendations according to their laboratory testing and finite element analysis results. These results, however, may not be appropriate for HA sections. More importantly, the existing standards—such as the Australian and New Zealand Standards (AS/NZ S4600) [30], American Iron and Steel Institute (AISI S100-16) [31], and Australian Standards (AS/NZS 1664.1) [32]—do not include design guidelines for evaluating the web buckling capacity of high-strength aluminum sections.

This study aimed to address these gaps through a comprehensive numerical analysis, and the web buckling performance of HA channel sections undergoing ETF loading was analyzed. This research was built upon the work of Alsanat et al. [23], but focused on HA sections instead of traditional aluminum alloys. Both material grades of AA-6086 and 7075-T6 were considered. The finite element (FE) models were developed and verified using the data obtained from laboratory testing. A parametric investigation was undertaken to examine the impact of various parameters on the web buckling performance of HA sections. Based on the outcomes of the numerical investigation, the accuracy of the latest design recommendations in the AS/NZ S4600 [30] and AS/NZS 1664.1 [32] was assessed. Moreover, this study presented new design calculations for evaluating the web buckling strength of HA channel sections through reliability analysis.

2. Material Characteristics of High-Strength Aluminum Alloys

2.1. 7075-T6 Aluminum Alloy

Zhi et al. [1] carried out 16 tensile coupon tests using the coupons cut from the flange and web of columns. Four different nominal thicknesses—which were 4, 5, 6, and 8 mm—were considered, and each thickness was tested four times.

An extensometer was employed to record strain during laboratory testing, which were carried out on a 1000 kN testing machine. Figure 2a depicts stress–strain curves related to aluminum alloy 7075-T6. Table 1 summarizes its crucial material characteristics, including the 0.2% proof stress ($f_{0.2}$), ultimate strength (f_u), and elongation after failure with an initial gauge length of 80 mm (δ), as well as variables in the two-stage Ramberg–Osgood model ($E_{0.2}$, n, and m).

Table 1. Material characteristics of specimens obtained from tensile coupon tests [1,2].

Grades	Thickness t_w/mm	Young's Modulus E_0/GPa	Yield Stress $\sigma_{0.2}$/MPa	Ultimate Stress σ_u/MPa	Elongation δ_f (%)	n	m
AA-6086 [2]	-	74.4	456	485	11.8	-	-
7075-T6 [1]	4.0	75.1	577	651	11.0	43.5	1.9
	5.0	74.5	513	596	11.25	37.8	2.5
	6.0	74.5	474	569	11.16	25.6	2.0
	8.0	74.8	582	647	9.72	56.4	1.9

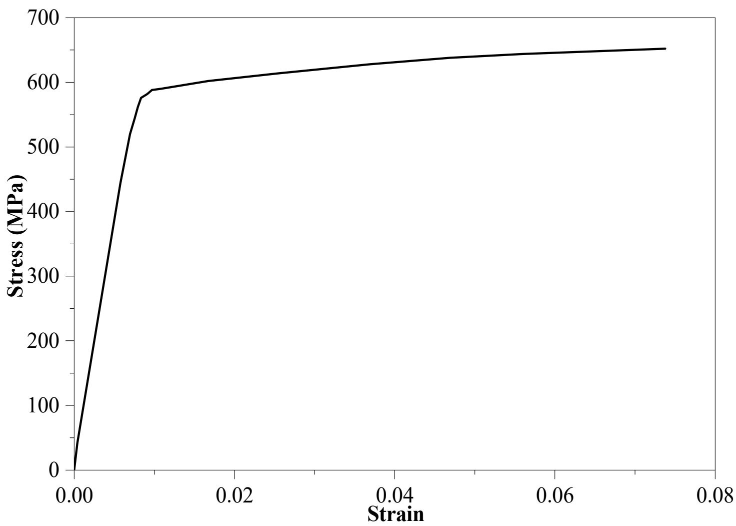

(**a**) 7075-T6 aluminum alloy

Figure 2. *Cont.*

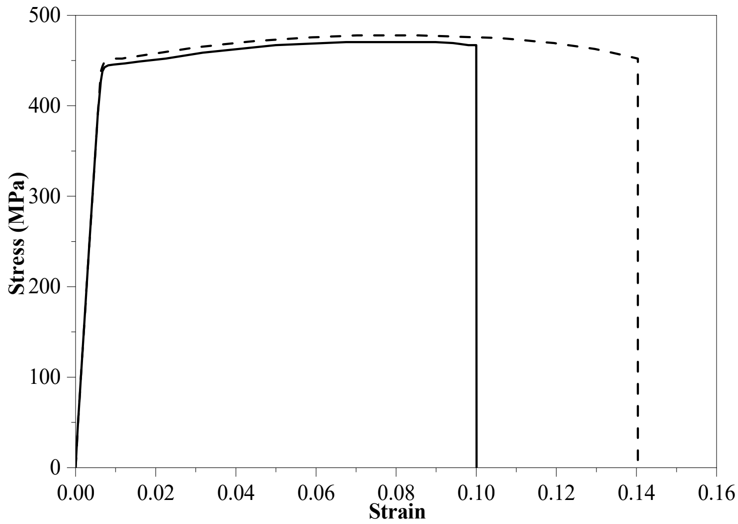

(**b**) AA-6086 aluminum alloy

Figure 2. Stress–strain curves of 7075-T6 [1] and AA-6086 [2].

2.2. AA-6086 Aluminium Alloy

Zupanič et al. [2] conducted two tensile coupon tests in order to characterize the physical properties of the aluminum alloy AA-6086. The new alloy had a higher silicon, copper, and zirconium content in its material composition. Before being analyzed, the material underwent the processes of being homogenized, extruded, and T6 heat-treated to achieve a desired state.

A mechanical extensometer featuring a 25 mm gauge length and a 100 kN servo-hydraulic test equipment was utilized. Figure 2b illustrates the stress–strain curves for the AA-6086 aluminum alloy and Table 1 summarizes its material properties.

3. Brief Overview of the Experimental Investigation [23]

3.1. General

Alsanat et al. [23] recently performed laboratory testing on web buckling for traditional aluminum alloy channels under ITF and ETF loadings. A total of forty test results were reported, which were then employed for validating the FE models. Detailed descriptions of both the laboratory testing and finite element models can be found in Alsanat et al. [23]; however, brief details concerning the laboratory testing methods are summarized below.

3.2. Testing Setup and Loading Process

All test specimens were manufactured from the structural aluminum alloy 5052H36. The depth of web section (*d*) was changed from 100 to 250 mm, while the widths of the flange (b_f) was changed from 60.5 to 75 mm. The specimen's total length (*L*) was calculated according to AS/NZ S4600 [30]. For the ITF condition, the length was calculated as being three times the height of the channel section added to the bearing plate length, and for the ETF condition, as being 1.5-times the height of the channel added together with the bearing plate length. The impact of bearing plate length on web buckling performance was evaluated (*N* was ranged from 25 mm to 150 mm). It should be noted that the flanges of these specimens were not fastened to the supports.

To carry out web buckling laboratory testing on the CFS sections, the procedures outlined in AS/NZ S4600 [30] were followed. Figure 3 shows the test setup, where a 100 kN Instron piece of testing equipment was utilized to exert a centralized reaction on the specimens. Half-rounds were employed to replicate the top and bottom hinge supports. The test specimens were positioned at the edge and mid-span between two bearing plates for the ETF and ITF loading case, respectively. Three laser displacement transducers (LVDTs) were employed to obtain the lateral displacement of the web in three different positions, while one LVDT was employed to obtain the vertical displacement of the bottom flange. Displacement control was implemented, maintaining a steady speed of 0.05 mm/min.

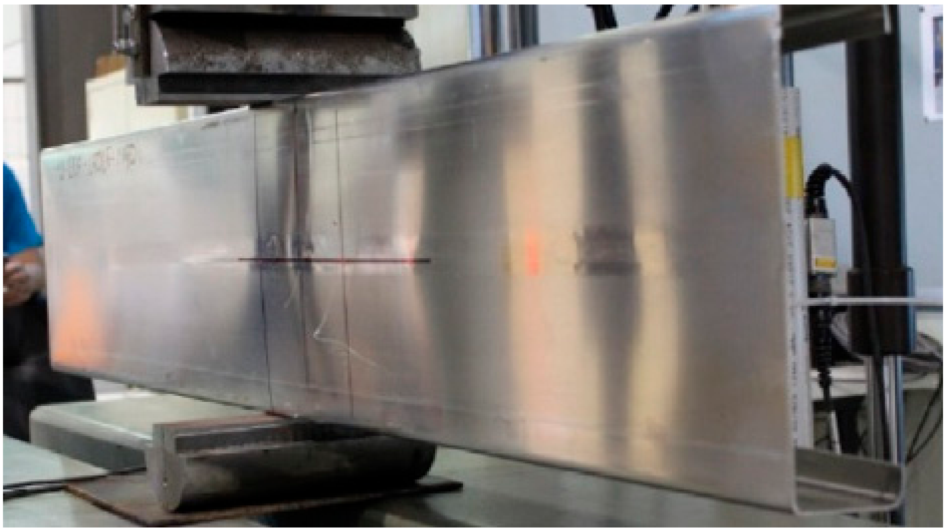

(**a**) ITF loading case

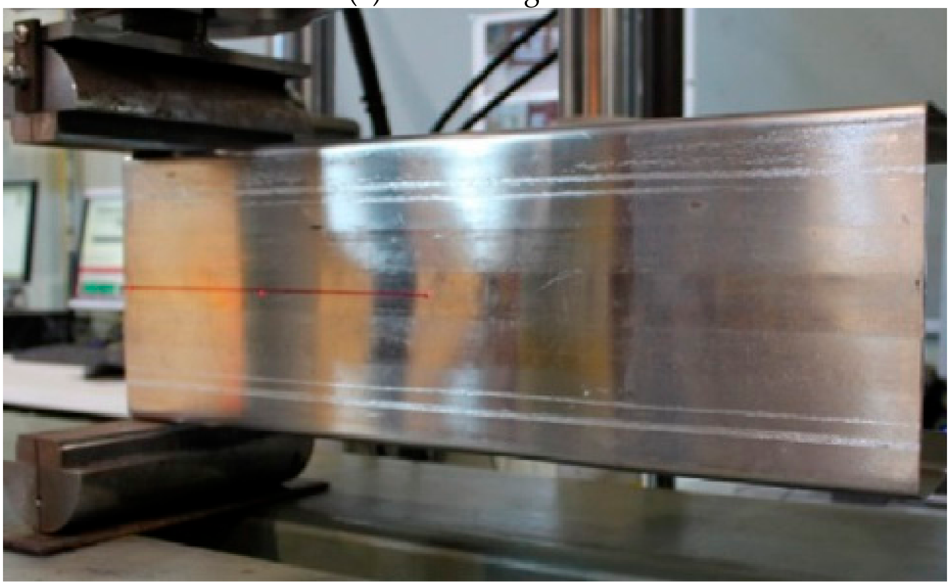

(**b**) ETF loading case

Figure 3. Testing setup for the web buckling tests [23].

4. Development of Numerical Models and Parametric Study

4.1. General

The ABAQUS software (Version 6.14-2) was employed to establish FE models that can simulate the nonlinear behavior and web buckling performance of HA channel sections. The recorded cross-sectional measurements and the aluminum's characteristics gleaned from the coupon tensile tests were adopted in the FE models. Similar modelling methods have been reported by many researchers [33–43]. A detailed discussion of the modelling method is presented as follows.

4.2. Geometry and Material Characteristics Modelling

In each analysis, the steel's isotropic yielding and plastic hardening were defined using the ABAQUS classical metal plasticity model. The stress–strain curve employed in the FE models was simplified, bilinear, and did not consider strain hardening. The numerical models incorporated the material parameters from coupon testing. The engineering material curve was transformed into an actual stress–strain curve in accordance with the recommended equations provided in the ABAQUS manual [44]. The true stress (σ_{true}) and true strain (ε_{true}) can be calculated by the following Equations (1) and (2):

$$\sigma_{true} = \sigma(1+\varepsilon) \quad (1)$$

$$\varepsilon_{true(pl)} = \ln(1+\varepsilon) - \frac{\sigma_{true}}{E} \quad (2)$$

4.3. FE Meshing

S4R shell elements were utilized to model channel sections made of the aluminum alloy, while the top and bottom endplates were simulated utilizing rigid quadrilateral shell elements (R3D4). In order to explore how various mesh sizes might impact the capacity of web buckling strength in these members, a mesh sensitivity analysis was undertaken, and the mesh size was varied from 2 mm to 50 mm. The impact of varying mesh element sizes on the ultimate strength of these sections has been studied, revealing that a mesh size of 5 mm was the suitable for simulating the aluminum alloy channel members—being able to provide accurate results. Mesh refinement was applied around the corner between the web and flange to achieve a more accurate FE analysis, as can be seen in Figure 4.

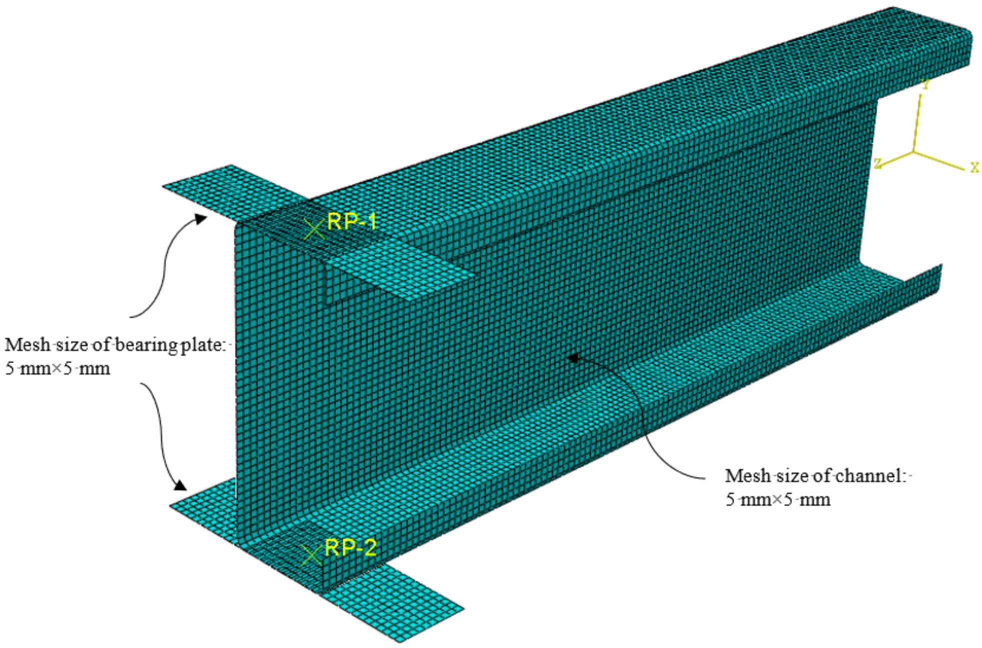

Figure 4. Mesh size employed in the FEMs.

4.4. Boundary Conditions and Loading Procedures

The boundary conditions deployed in the FE models are illustrated in Figure 5. The load in the axial direction was introduced via the reference point of the upper base plate using the displacement control general static method [44]. All degrees of freedom on the top surface of the end plates were constrained except for translational flexibility in the Y axis. The surface-to-surface contact option was selected in the modelling of the interface between the end plates and the aluminum alloy section. No object was allowed to pass through these two touching surfaces.

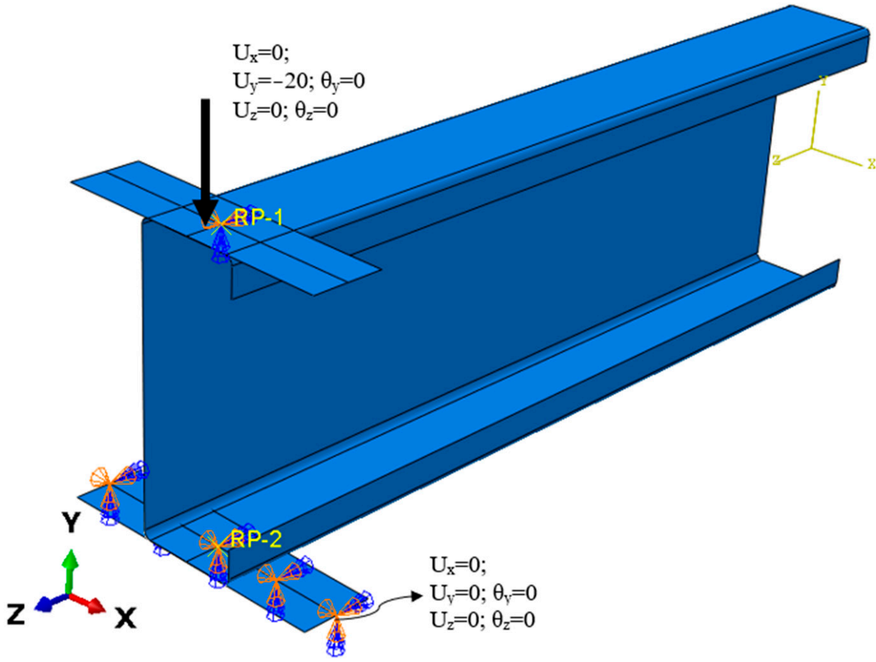

Figure 5. Boundary conditions applied in the FEMs.

4.5. Analysis Methods

Elastic buckling and implicit dynamic analysis were employed to model the aluminum alloy channel sections. The dynamic approach involving implicit time integration was utilized to determine the models' quasi-static responses.

4.6. FE Model Validation

A total of 19 laboratory test outcomes for aluminum-lipped channel sections presented by Alsanat et al. [23] were included in Table 2 to validate the numerical modelling methodology adopted in this investigation. Figure 6 depicts the failure modes seen in laboratory testing and FE analysis. It can be observed that the shapes of deformation suggested by the FE models were comparable to the ones discovered through the laboratory testing. Table 2 contrasts the experimental data (P_{EXP}) with the computational findings (P_{FEA}). As displayed in Figure 7, the P_{EXP}/P_{FEA} had a coefficient of variation of 0.09 and a mean of 0.98, showing that the web buckling strength of aluminum alloy channels could be reliably estimated using the FE models developed in this work. Figure 8 presents the load–displacement curves generated from the numerical modelling and laboratory testing, demonstrating a strong agreement.

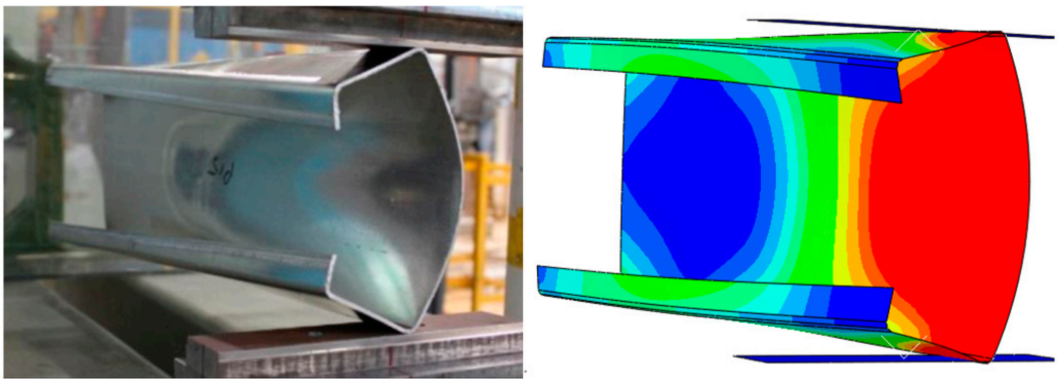

Figure 6. Comparison between failure modes from the laboratory testing [23] and numerical analysis (ETF-20025-N50).

Table 2. Comparison of the ultimate strength predicted from laboratory tests [23] and numerical analysis.

Specimen ID	Web	Flange	Lip	Thickness	Length	Bearing Width	Test Result	FEA Result	P_{TEST}/P_{FEA}
	h_w	b_f	l_b	t	L	N	P_{TEST}	P_{FEA}	
	(mm)	(mm)	(mm)	(mm)	(mm)	(mm)	(kN)	(kN)	
ETF-10030-N25	107.3	60.4	14.9	2.95	316	25	6.19	5.44	1.14
ETF-10030-N50	106.5	58.4	16.1	2.95	317	50	6.23	6.26	1.00
ETF-10030-N100	107.3	59.4	15.0	2.95	316	100	7.41	8.40	0.88
ETF-15030-N25	156.7	62.8	22.9	2.93	466	25	5.23	5.23	1.00
ETF-15030-N50	157.5	63.3	22.4	2.93	465	50	5.5	6.07	0.91
ETF-15030-N100	158.3	63.5	21.7	2.92	465	100	6.37	6.70	0.95
ETF-15030-N150	155.5	63.5	22.9	2.92	467	150	7.25	8.80	0.82
ETF-20025-N25	208.1	74.6	25.5	2.42	617	25	3.33	3.19	1.04
ETF-20025-N50	208.1	74.2	25.4	2.43	615	50	3.61	3.55	1.02
ETF-20025-N100	207.3	74.3	25.7	2.43	615	100	3.92	4.10	0.96
ETF-20025-N150	201	75.8	26.5	2.43	615	150	4.23	4.70	0.90
ETF-20030-N25	204.6	74.9	27.4	2.9	611	25	4.95	4.80	1.03
ETF-20030-N50	208.4	73	27.5	2.9	615	50	5.07	5.21	0.97
ETF-20030-N100	204.5	75.4	27.5	2.89	613	100	5.82	6.28	0.93
ETF-20030-N150	208.3	73.5	27.1	2.89	615	150	6.06	7.50	0.81
ETF-25025-N25	259.8	80.8	23.4	2.43	765	25	2.95	2.83	1.04
ETF-25025-N50	259.9	76.1	23.7	2.44	765	50	3.09	3.06	1.01
ETF-25025-N100	262.1	76.2	22.7	2.44	765	100	3.76	3.53	1.07
ETF-25025-N150	260.3	76.3	23.4	2.45	765	150	4.15	3.84	1.08
Mean									0.98
COV									0.09

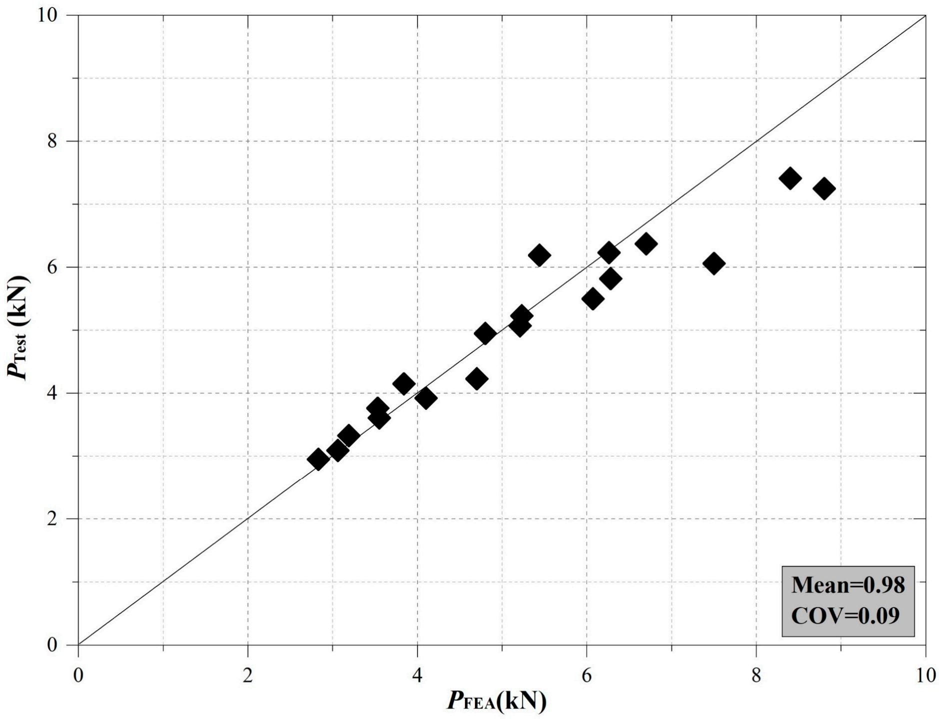

Figure 7. Comparison of ultimate strength between the laboratory tests [23] and numerical analysis.

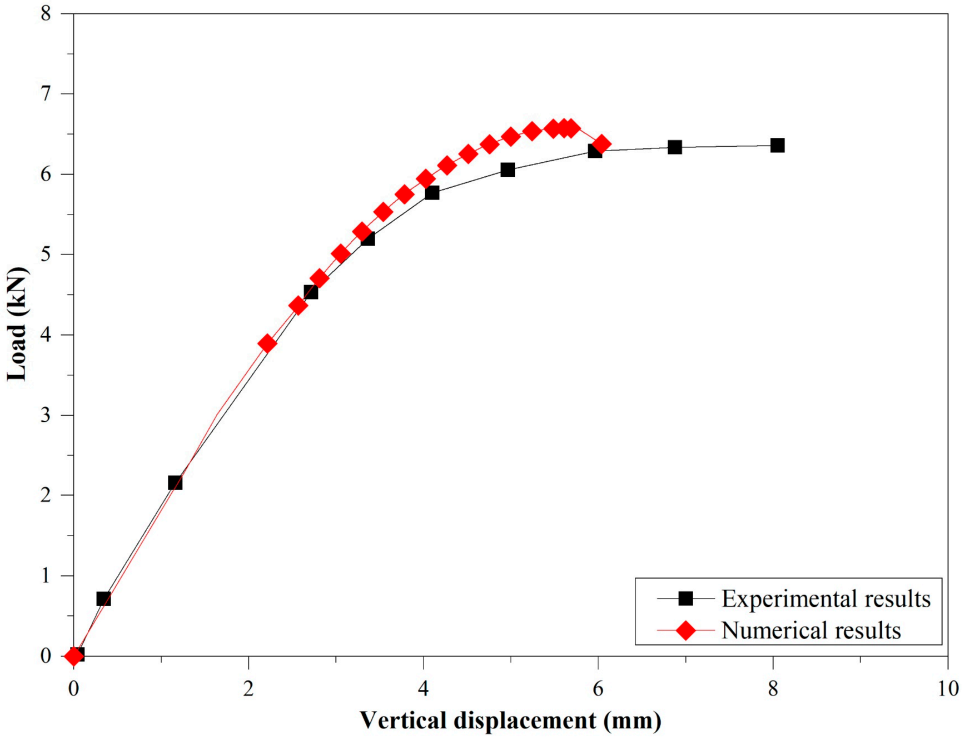

(**a**) ETF-15030-N100

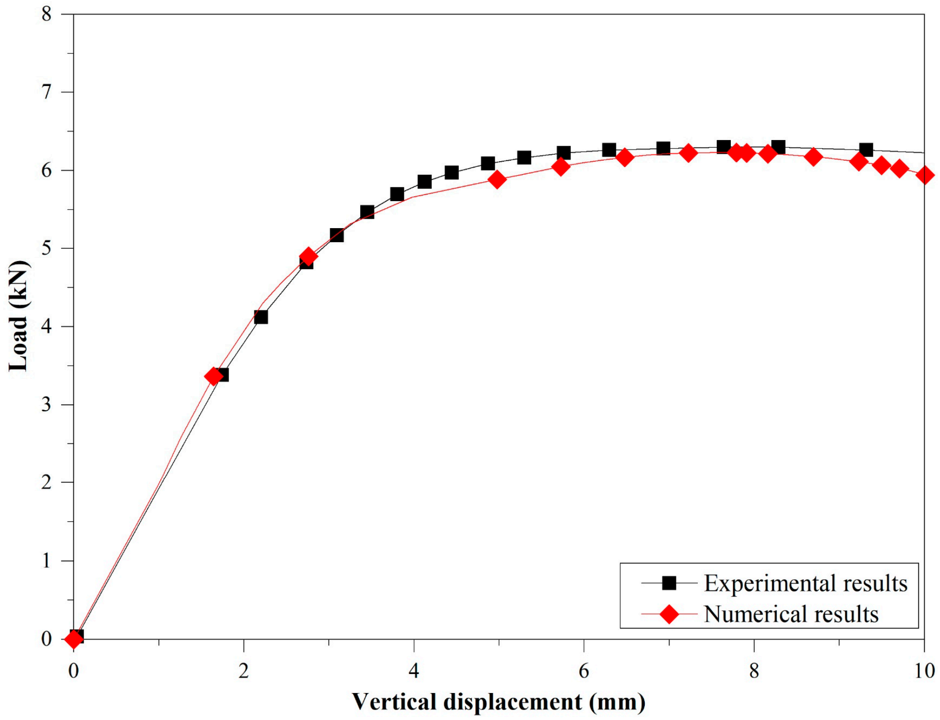

(**b**) ETF-10030-N50

Figure 8. Load-displacement relationship between the laboratory tests [23] and numerical analysis.

4.7. Parametric Study for High-Strength Aluminum Alloys

After the verification of the FE models for conventional aluminum alloy channel sections, a detailed parametric investigation was undertaken to create a comprehensive database for HA sections. A total of 1024 simulation results were generated, in which 256 FE results were for AA-6086 aluminum alloy lipped channel sections, 256 FE results were for AA-6086 aluminum alloy unlipped channel sections, 256 FE results were for

7075-T6 aluminum alloy lipped channel sections, and the remaining 256 FE results were for 7075-T6 aluminum alloy unlipped channel sections.

Previous work reported by Chen et al. [29] demonstrated that the web buckling strength of CFS sections is primarily affected by the length of the bearing plate (*N*), web slenderness ratio (h/t_w), and internal corner radii ratio (r_i/t_w). Therefore, a wide range of HA sections covering varying web slenderness ratios, internal corner radii, bearing lengths, and aluminum alloy grades were examined in the parametric study (Table 3). The web slenderness ratio (h/t_w) was considered at values of 50, 75, 100, and 125. Four bearing plate lengths (*N*) were selected: 25, 50, 75, and 100 mm. The internal corner radii ratio (r_i/t_w) was considered at values of 1.0, 2.0, 3.0, and 4.0. Four distinct web thicknesses of aluminum alloy channels (t_w) were included in the parametric study—namely, 1.0, 2.0, 3.0, and 4.0 mm.

Table 3. Details of the parametric analysis.

Key Parameters	Range	Quantity
web slenderness ratio (h/t_w)	50, 75, 100, 125	512
bearing plates (*N*)	25 mm, 50 mm, 75 mm, 100 mm	512
internal corner radii ratio (r_i/t_w)	1.0, 2.0, 3.0, 4.0	512
web thickness (t_w)	1.0 mm, 2.0 mm. 3.0 mm, 4.0 mm	512
lip conditions	lipped, unlipped	1024
material grade	7075-T6, AA-6086	1024

Figures 9–11 show the impact of the ratios h_w/t, N/t, and r_i/t on the web buckling strength of HA sections, correspondingly. When h_w/t rose from 50 to 125, a minor reduction in strength was noticed—as illustrated in Figure 9. As depicted in Figure 10, the web buckling strength increased significantly when N/t increased from 25 to 100. The impact of the r/t ratio on the web buckling strength of the HA sections was studied, as illustrated in Figure 11, and it was found that a considerable decrease in strength was observed when r/t increased from 1.0 to 4.0. This indicated that the impact of the r/t ratio on the web buckling strength cannot be ignored.

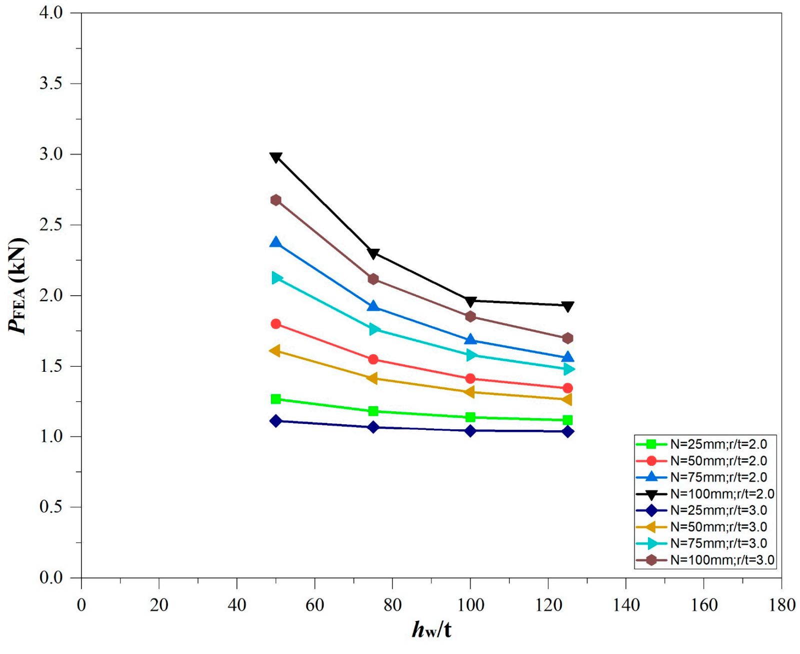

(**a**) 7075-T6 (lipped channels)

Figure 9. *Cont.*

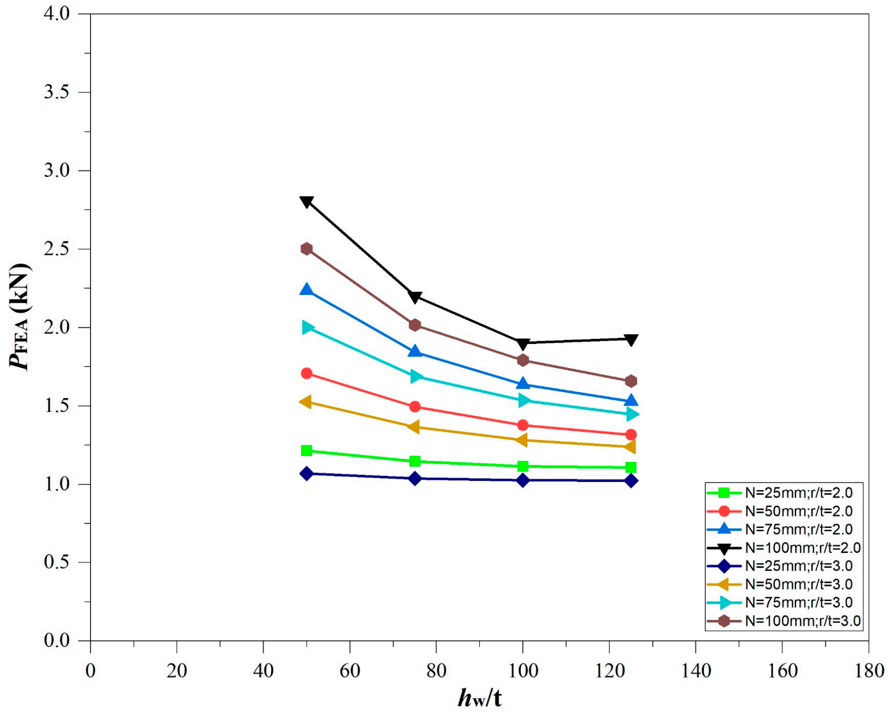

(**b**) AA-6086 (lipped channels)

Figure 9. Web buckling strength versus web stiffness ratio (h_w/t).

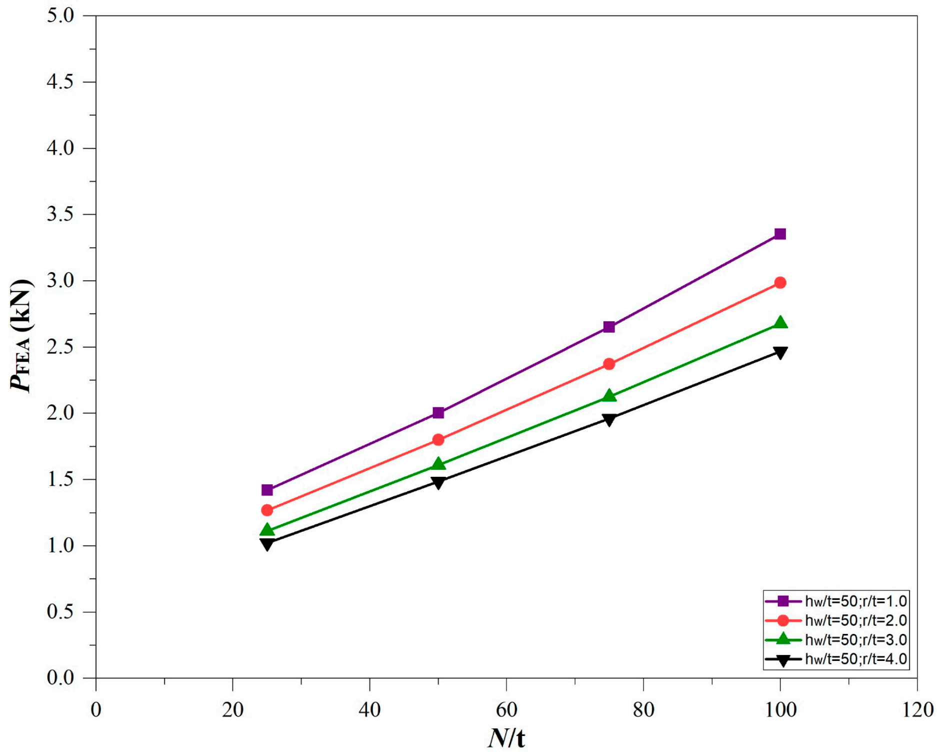

(**a**) 7075-T6 (lipped channels)

Figure 10. *Cont.*

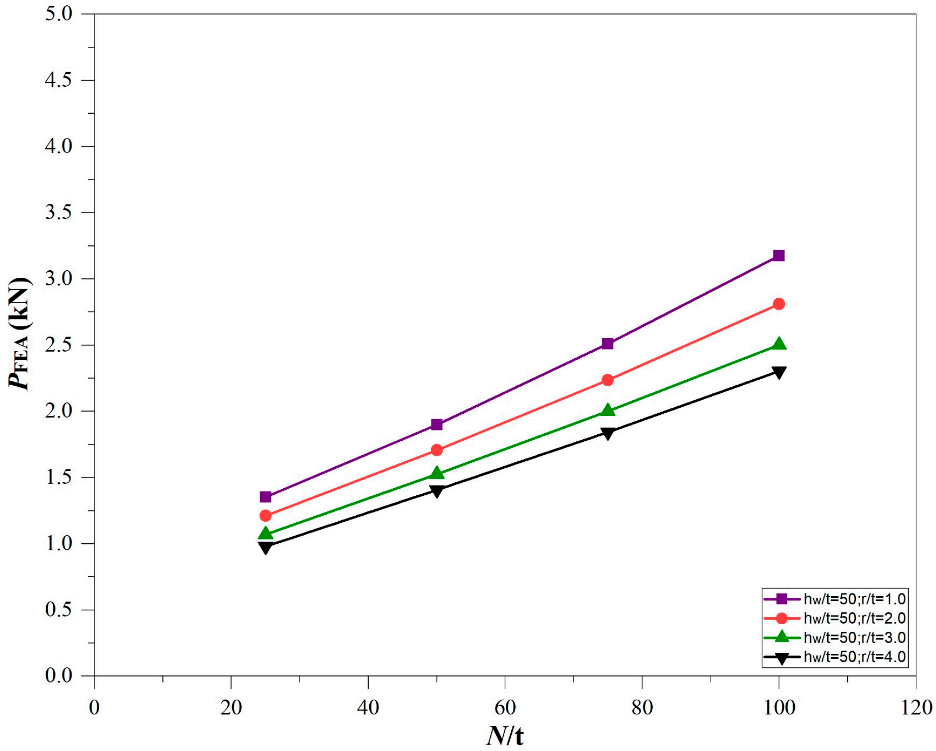

(**b**) AA-6086 (lipped channels)

Figure 10. Web buckling strength versus the bearing length ratio (N/t).

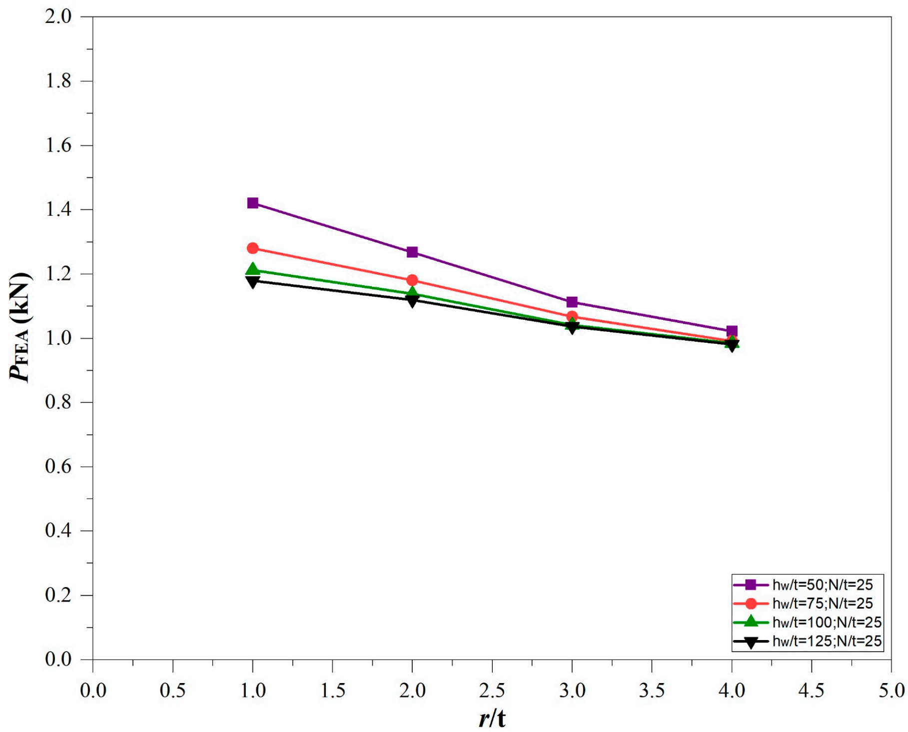

(**a**) 7075-T6 (lipped channels)

Figure 11. *Cont.*

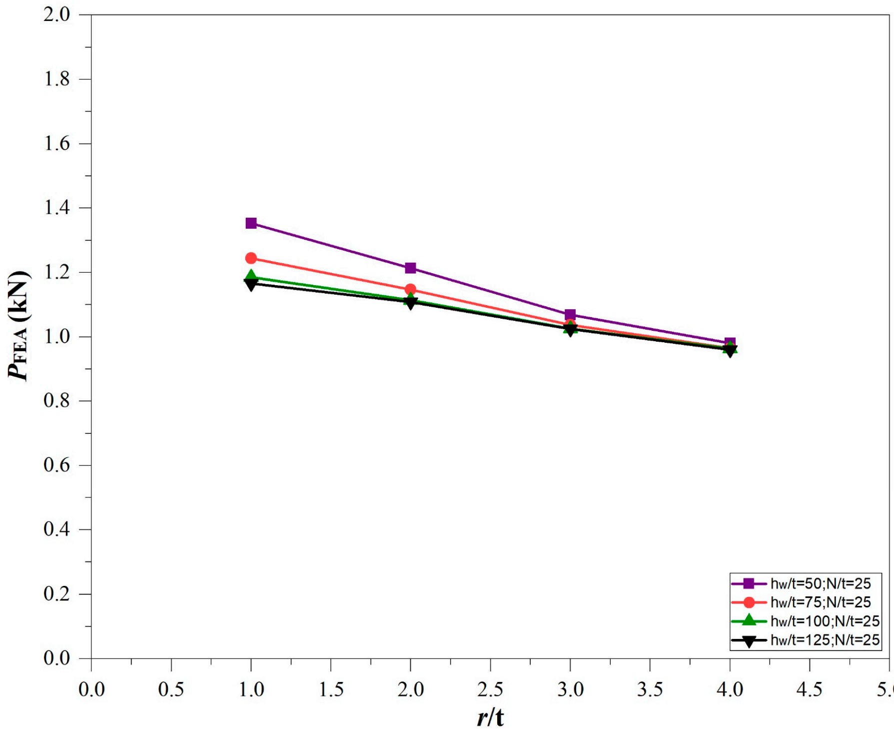

(**b**) AA-6086 (lipped channels)

Figure 11. Web buckling strength versus the inside bent radius ratio (r/t).

5. Evaluation of the Current Design Guidelines

5.1. General

The web buckling strength database derived from the parametric analysis was evaluated against the expected web buckling strength calculated by the latest design recommendation given in AS/NZS 4600 [30] and AS/NZS 1664.1 [32]. AS/NZS 4600 [30] is intended for cold-formed carbon steel, while AS/NZS 1664.1 [32] is a specification for aluminum buildings. It is worth mentioning that the comparison mentioned does not consider the design methods outlined in Eurocode 9 [45] for aluminum structures. These methods are applicable only to aluminum structural sheeting, which involves members with two or more webs. They do not provide design guidelines for determining the web buckling strength of single-web sections such as aluminum channel sections. Additionally, a recent study by Alsanat et al. [23] found that Eurocode 9 [45] was not suitable for estimating the web buckling strength of aluminum single-web sections.

5.2. Design Methods in AS/NZ S4600 [30]

The current AS/NZ S4600 [30] and AISI S100-16 [31] guidelines provide design calculations with different specific coefficients for evaluating the web buckling strength of CFS lipped channels. These coefficients are directly related to the loading conditions, types of support, and flange types. The expression for evaluating the web buckling strength is as illustrated below:

$$R_b = Ct_w^2 f_y \sin\theta \left(1 - C_w\sqrt{\frac{h}{t_w}}\right)\left(1 - C_r\sqrt{\frac{r_i}{t_w}}\right)\left(1 + C_l\sqrt{\frac{N}{t_w}}\right) \quad (3)$$

5.3. Design Methods in AS/NZS 1664.1 [32]

Design calculations are available in AS/NZS 1664.1 [32] for estimating the web buckling strength of aluminum alloy channel sections undergoing ETF and ITF loadings. Additionally, any enhancement in web buckling strength due to the flanges secured to the supports is disregarded in the design guidelines. The design calculations for both flange-fastened and unfastened support scenarios are the same. Below is the expression for estimating the web buckling strength under ETF and ITF loading:

$$P_{AS1664} = (1.2t_w^2 \sin\theta(0.46f_y + 0.02\sqrt{Ef_y})(N + C_{w2}))/(C_{w3} + r_i(1 - \cos\theta)) \quad (4)$$

$$P_{AS1664} = (t_w^2 \sin\theta(0.46f_y + 0.02\sqrt{Ef_y})(N + C_{w1}))/(C_{w3} + r_i(1 - \cos\theta)) \quad (5)$$

5.4. Comparing the Design Strengths with the Simulation Results

In this section, the accuracy of the existing design methods given in AS/NZ S4600 [30] and AS/NZS 1664.1 [32] were evaluated based on the parametric analysis outcomes.

The design strengths derived from AS/NZ S4600 [30] and AS/NZS 1664.1 [32] were compared to the web buckling strength obtained from the parametric investigation. The comparison was summarized in Table 4. As illustrated in Figure 12, the average design strength calculated by AS/NZ S4600 [30] compared to the simulation results was 1.53 and 1.37 for 7075-T6 and AA-6086, respectively. The web buckling strength predicted by AS/NZS 1664.1 [32] was slightly unconservative by 14% and 2% for 7075-T6 and AA-6086, respectively, compared to simulation results (see Figure 13). This indicates that the existing design methodologies tend to be overly conservative when assessing the web buckling strength of such members.

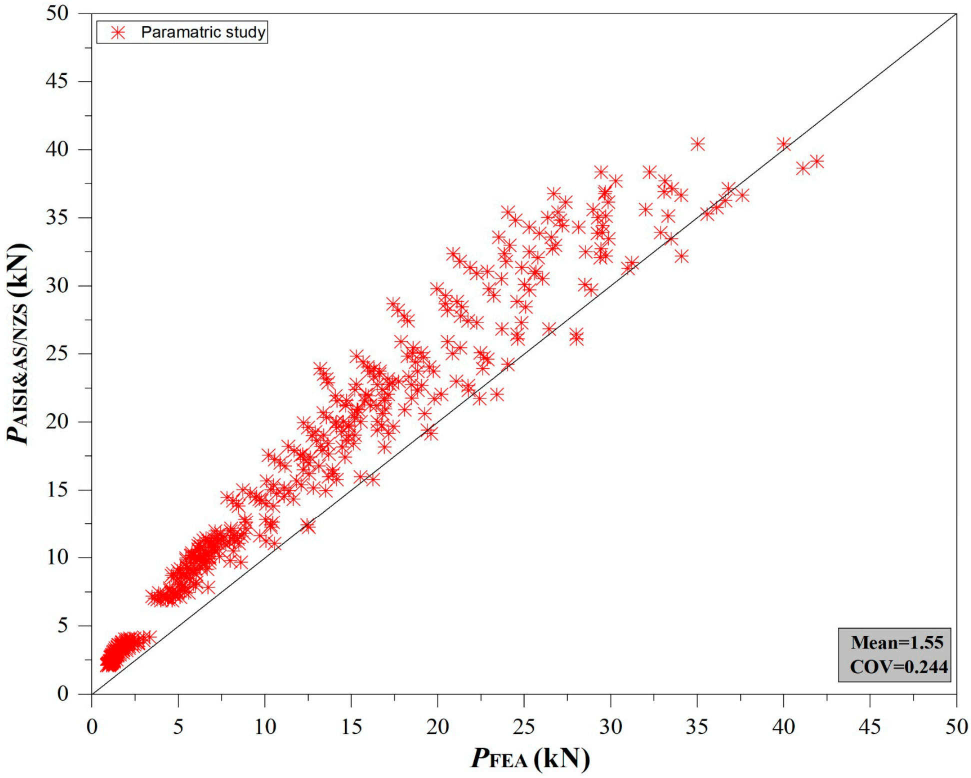

(**a**) 7075-T6

Figure 12. *Cont.*

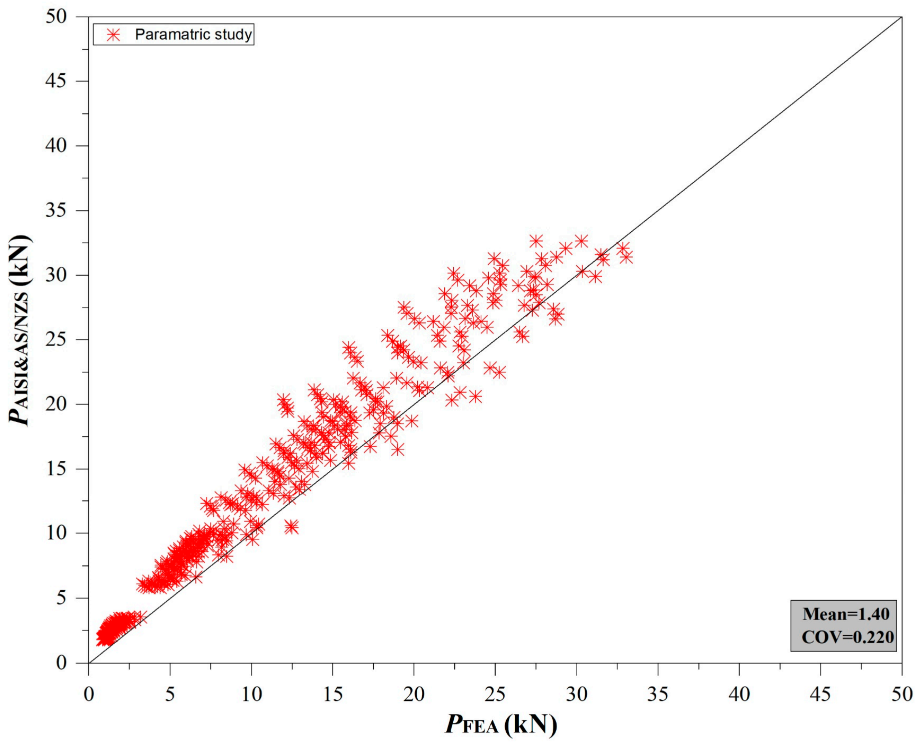

(**b**) AA-6086

Figure 12. Comparison between simulation results and design strength calculated by AS/NZS 4600 [30].

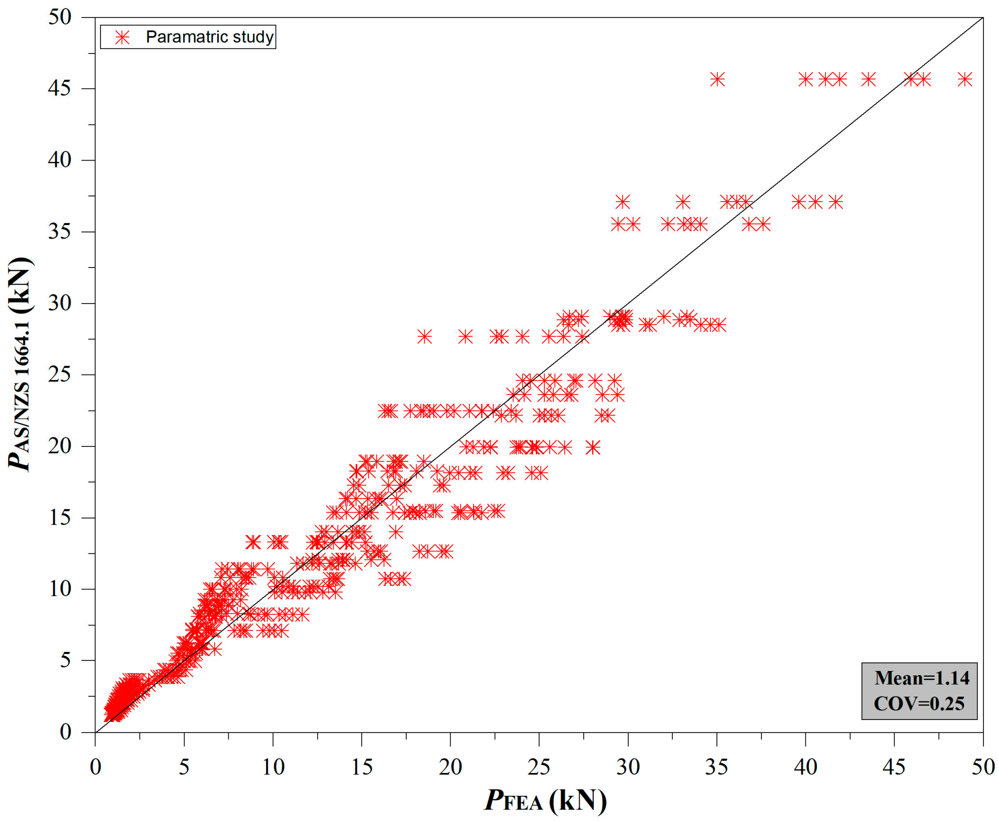

(**a**) 7075-T6

Figure 13. *Cont.*

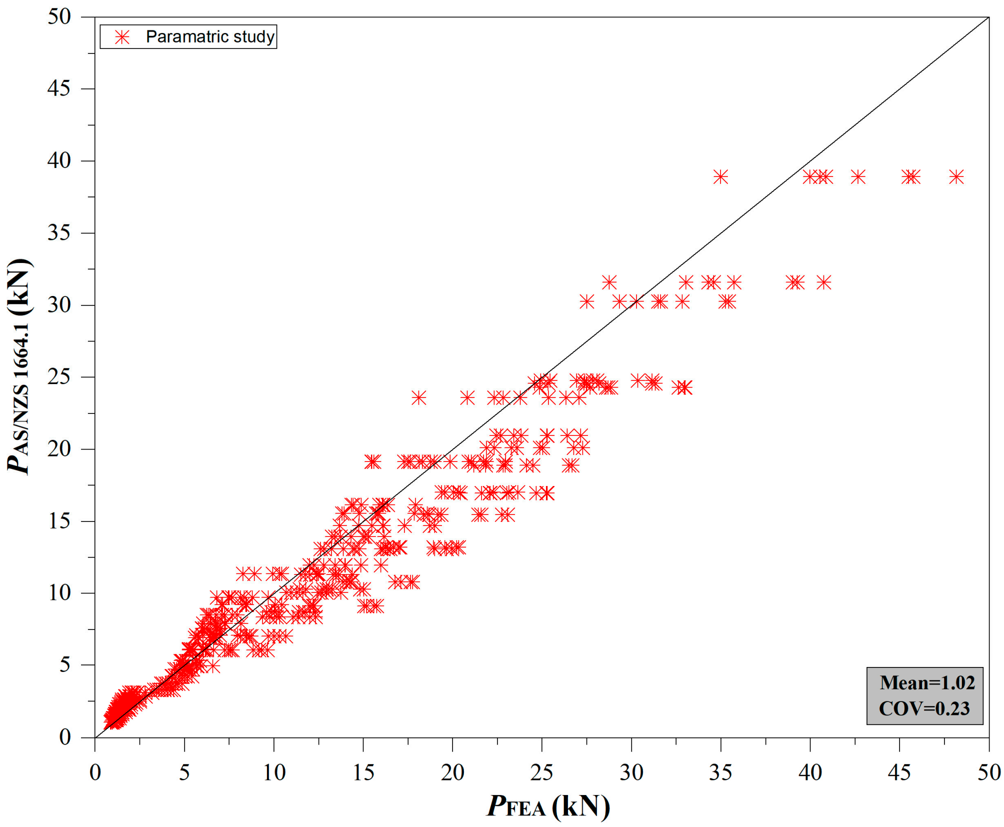

(**b**) AA-6086

Figure 13. Comparison between the simulation results and design strength calculated by AS/NZS 1664.1 [32].

Table 4. Comparison of the simulation results with the design strength.

	Existing Design Proposals/Parametric Study Results				New Design Proposals/Parametric Study Results	
	AS/NZ S4600 [30]		AS/NZS 1664.1 [32]		M-AS/NZ S4600	
	7075-T6	AA-6086	7075-T6	AA-6086	7075-T6	AA-6086
Mean	1.53	1.37	1.14	1.02	0.94	0.93
COV	0.25	0.24	0.25	0.23	0.24	0.25
β					2.51	2.50

6. Proposed Design Equations for High-Strength Aluminum Alloys

6.1. Development of New Design Equations (M-AS/NZ S4600)

As mentioned previously, the existing design rules are demonstrated to be over conservative when assessing the web buckling strength of such members, and new design rules should be presented in this investigation. The simulation results suggested that the impact of the h_w/t, N/t, and r_i/t ratios on the web buckling strength of HA sections was significant. This indicates the importance of including the impact of h_w/t, N/t, and r_i/t ratios when proposing design calculations for estimating the web buckling strength of such members.

In this investigation, new design calculations were presented based on three key parameters (h_w/t, N/t, and r_i/t ratios), which followed the format of the design calculations given in AS/NZS 4600 [30]. Therefore, only new coefficients such as 1.483, 0.01, 0.265, and 0.505 were developed using the bivariate linear regression analysis, based on a total of 1024 numerical results. Table 5 summarizes the new coefficients for HA presented in this work. The web buckling capacity (Rb) for 7075-T6 and AA-6086 HA can be determined from Equations (6)–(9):

For 7075-T6 lipped channel sections:

$$R_b = 1.483t_w^2 f_y \sin\theta \left(1 - 0.01\sqrt{\frac{h}{t_w}}\right)\left(1 - 0.265\sqrt{\frac{r_i}{t_w}}\right)\left(1 + 0.505\sqrt{\frac{N}{t_w}}\right) \tag{6}$$

For 7075-T6 unlipped channel sections:

$$R_b = 1.495t_w^2 f_y \sin\theta \left(1 - 0.01\sqrt{\frac{h}{t_w}}\right)\left(1 - 0.274\sqrt{\frac{r_i}{t_w}}\right)\left(1 + 0.433\sqrt{\frac{N}{t_w}}\right) \tag{7}$$

For AA-6086 lipped channel sections:

$$R_b = 1.492t_w^2 f_y \sin\theta \left(1 - 0.01\sqrt{\frac{h}{t_w}}\right)\left(1 - 0.281\sqrt{\frac{r_i}{t_w}}\right)\left(1 + 0.626\sqrt{\frac{N}{t_w}}\right) \tag{8}$$

For AA-6086 unlipped channel sections:

$$R_b = 1.516t_w^2 f_y \sin\theta \left(1 - 0.01\sqrt{\frac{h}{t_w}}\right)\left(1 - 0.289\sqrt{\frac{r_i}{t_w}}\right)\left(1 + 0.533\sqrt{\frac{N}{t_w}}\right) \tag{9}$$

Table 5. Coefficients of the proposed design equation.

	Proposed Coefficients				Limits
	C	C_r	C_l	C_w	
7075-T6 aluminium alloy					
Lipped channel sections	1.483	0.265	0.505	0.01	$1 \le r/t \le 4$, $25 \le N \le 100$,
Unlipped channel sections	1.495	0.274	0.433	0.01	$50 \le h/t \le 125$, θ = 90°
AA-6086 aluminium alloy					
Lipped channel sections	1.492	0.281	0.626	0.01	$1 \le r/t \le 4$, $25 \le N \le 100$,
Unlipped channel sections	1.516	0.289	0.533	0.01	$50 \le h/t \le 125$, θ = 90°

These equations are limited to HA channel sections with dimensional ranges of $1 \le r/t \le 4$, $25 \le N \le 100$, $50 \le h/t \le 125$, and θ = 90°.

As depicted in Figure 14, the simulation results—which were the outcomes from the parametric investigation—and the design strengths, which were derived from the newly presented equations given in this investigation (M-AS/NZ S4600), were comparatively analyzed. Table 4 summarizes the findings from the comparison. The average ratio of design values to simulation results was found to be 0.94, and the coefficient of variation (COV) was 0.24 for 7075-T6 aluminum, while the average ratio was 0.93 and the COV was 0.25 for AA-6086 aluminum. Therefore, it can be concluded that the newly presented design calculations provided in this research (M-AS/NZ S4600) were marginally conservative in comparison to the simulation results.

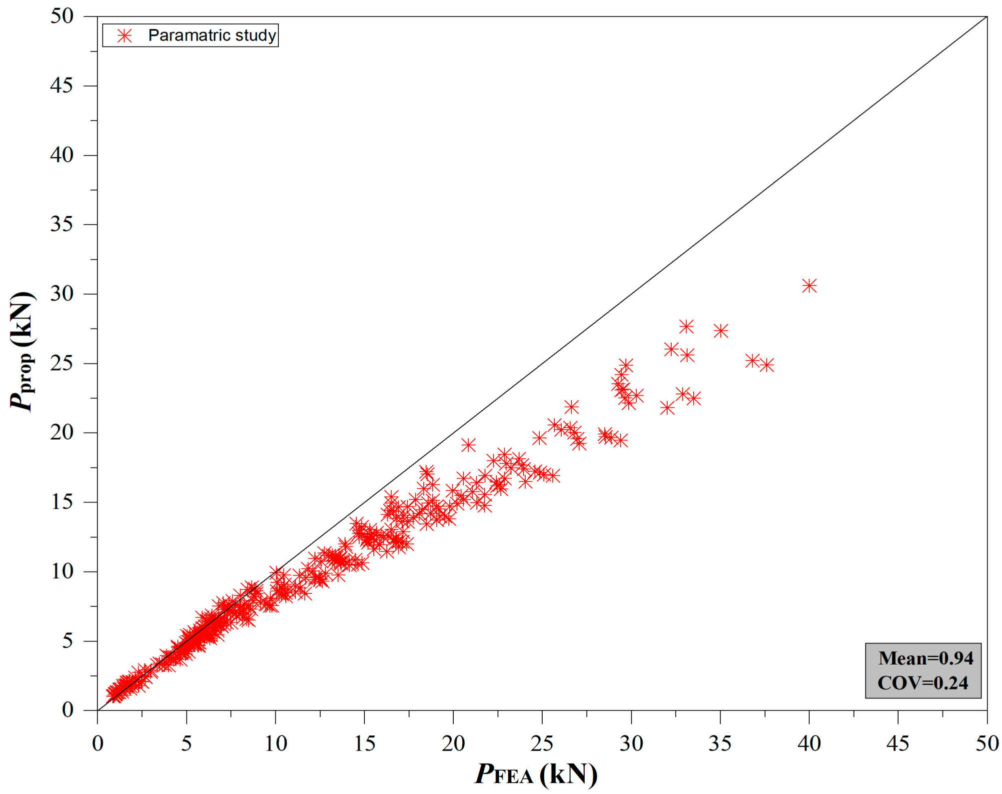

(**a**) 7075-T6

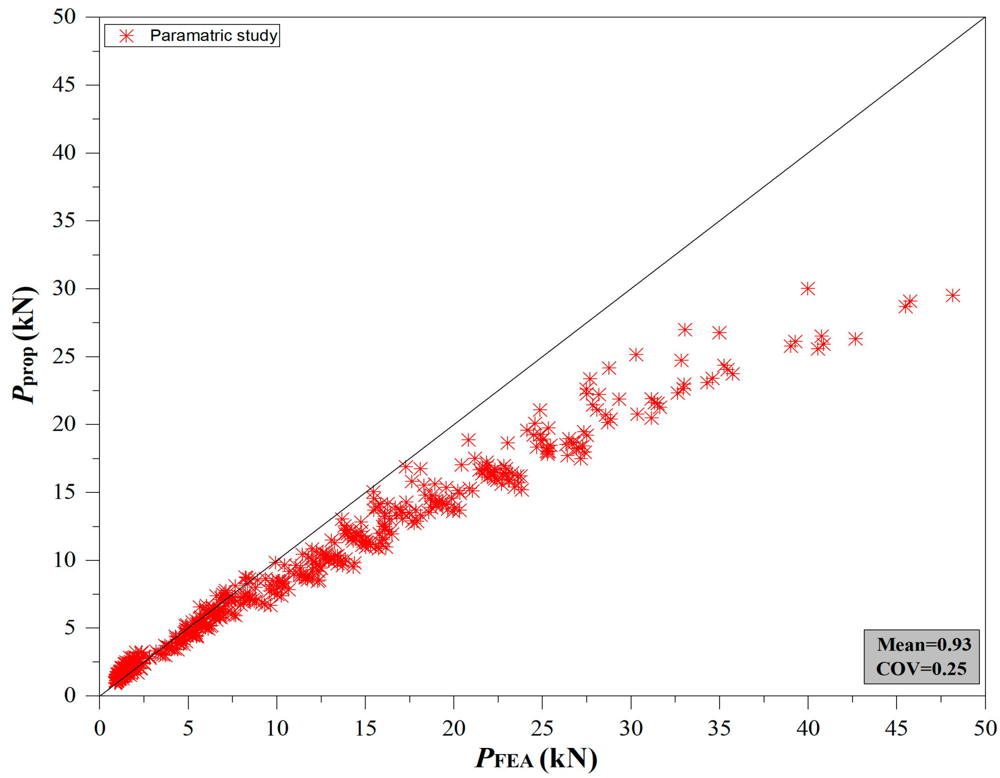

(**b**) AA-6086

Figure 14. Comparison between the simulation results and design strength calculated by proposed design formulas.

6.2. Reliability Analysis

A reliability assessment was undertaken to determine the accuracy of the newly developed design calculations in web buckling, and the reliability of the proposed formulae was evaluated based on the statistical model recommended by the AS/NZ S4600 [30] and AISI S100-16 [32]:

$$\varphi_w = 11.5 M_m F_m P_m e^{-\beta\sqrt{V_m^2+V_F^2+C_n V_P^2+V_Q^2}} \quad (10)$$

As per AS/NZ S4600 [30] and AISI S100-16 [32], a reliability index (β) value of at least 2.5 indicates reliable design calculations. During the reliability analysis, a loading condition of 1.2DL + 1.6LL was chosen, where DL stands for dead load and LL for live load. The statistical parameters chosen for the material and fabrication properties were based on the averages (M_m = 1.10, F_m = 1.00) and COVs (V_M = 0.10, V_F = 0.05) in accordance with AS/NZ S4600 [30] and AISI S100-16 [32]. According to Table 4, the values of β were found to be 2.51 and 2.50 for 7075-T6 and AA-6086, respectively, implying that the suggested design method can properly estimate the web buckling strength of such members. More information regarding the reliability analysis is available in AS/NZ S4600 [30] and AISI S100-16 [32].

7. Conclusions

This study focused on the web buckling performance of high-strength aluminum alloy channel sections subjected to end-two-flange (ETF) loading. Both material grades of AA-6086 and 7075-T6 were investigated. Based on the outcomes of this study, the following conclusions can be drawn:

(1) A parametric investigation consisting of 1024 models was performed using the finite element (FE) models previously developed for traditional aluminum alloys. A wide range of high-strength aluminum alloy sections covering varying web slenderness ratios, internal corner radii, bearing lengths, and aluminum alloy grades were considered. The results obtained from the parametric investigation suggested that the impact of h_w/t, N/t, and r_i/t ratios on the web buckling strength of high-strength aluminum alloy sections was significant. This indicates the importance of including the impact of h_w/t, N/t, and r_i/t ratios when proposing the design calculations for estimating the web buckling strength of such members.

(2) The accuracy of the latest design recommendations provided in the Australian and New Zealand Standards (AS/NZ S4600; 2018) and Australia Standards (AS/NZS 1664.1; 1997) was evaluated by comparing them with the parametric analysis results. The results showed that the average design strength calculated by AS/NZ S4600 to the simulation results was 1.53 and 1.37 for 7075-T6 and AA-6086, respectively. The web buckling strength predicted by AS/NZS 1664.1 was slightly unconservative by 14% and 2% for 7075-T6 and AA-6086, respectively, compared to the simulation results. It was shown that the latest design recommendations were over-conservative when estimating the web buckling strength of such channel sections.

(3) Four unified web buckling equations with new coefficients for high-strength aluminum alloys were presented based on the simulation results. The same methodology as AS/NZS 4600 (2018) was adopted in developing the new design calculations. The average ratio of design values to simulation results was found to be 0.94, and the coefficient of variation (COV) was 0.24 for 7075-T6 aluminum, while the average ratio was 0.93 and the COV was 0.25 for AA-6086 aluminum. A comparison revealed that the design strengths calculated by the newly presented formulas (M-AS/NZ S4600) were close to the simulation results.

(4) The accuracy of the new design calculations presented in this work were evaluated through a reliability analysis. The reliability index values (β) for 7075-T6 and AA-6086 were determined to be 2.51 and 2.50, respectively, indicating that the new design calculations can closely estimate the web buckling strength of such channel sections.

(5) Although an extensive parametric investigation has been undertaken, an experimental program should be performed to evaluate the accuracy of the design calculations presented in this investigation.

Author Contributions: Conceptualization, G.S.; methodology, X.-Y.S.; software, J.-H.F. All authors have read and agreed to the published version of the manuscript.

Funding: This research received no external funding.

Data Availability Statement: The data used to support the findings of this study are available from the corresponding author upon request.

Conflicts of Interest: The authors declare no conflict of interest.

References

1. Zhi, X.; Wang, Y.; Zhang, Y.; Li, B.; Ouyang, Y. Study of local buckling performance of 7075-T6 high-strength aluminium alloy H-section stub columns. *Thin-Walled Struct.* **2022**, *180*, 109925. [CrossRef]
2. Zupanič, F.; Klemenc, J.; Steinacher, M.; Glodež, S. Microstructure, mechanical properties and fatigue behaviour of a new high-strength aluminium alloy AA 6086. *J. Alloys Compd.* **2023**, *941*, 168976. [CrossRef]
3. Li, B.; Wang, Y.; Zhang, Y.; Meng, X.; Yuan, H.; Zhi, X. Flexural buckling of extruded high-strength aluminium alloy SHS columns. *Thin-Walled Struct.* **2022**, *179*, 109717. [CrossRef]
4. Fang, Z.; Roy, K.; Xu, J.; Dai, Y.; Paul, B.; Lim, J.B.P. A novel machine learning method to investigate the web crippling behaviour of perforated roll-formed aluminium alloy unlipped channels under interior-two flange loading. *J. Build. Eng.* **2022**, *51*, 104261. [CrossRef]
5. Roy, K.; Chen, B.; Fang, Z.; Uzzaman, A.; Chen, X.; Lim, J.B.P. Local and distortional buckling behaviour of back-to-back built-up aluminium alloy channel section columns. *Thin-Walled Struct.* **2021**, *163*, 107713. [CrossRef]
6. Roy, K.; Chen, B.; Fang, Z.; Uzzaman, A.; Lim, J.B.P. Axial capacity of back-to-back built-up aluminium alloy channel section columns. *J. Struct. Eng.-ASCE* **2022**, *148*, 04021265. [CrossRef]
7. Fang, Z.; Roy, K.; Chen, B.; Xie, Z.; Ingham, J.; Lim, J.B.P. Effect of the web hole size on the axial capacity of back-to-back aluminium alloy channel section columns. *Eng. Struct.* **2022**, *260*, 114238. [CrossRef]
8. Fang, Z.; Roy, K.; Chen, B.; Xie, Z.; Lim, J.B.P. Local and distortional buckling behaviour of aluminium alloy back-to-back channels with web holes under axial compression. *J. Build. Eng.* **2022**, *47*, 103837. [CrossRef]
9. Feng, R.; Chen, Z.; Shen, C.; Roy, K.; Chen, B.; Lim, J.B.P. Flexural capacity of perforated aluminium CHS tubes—An experimental study. *Structures* **2020**, *25*, 463–480. [CrossRef]
10. Uzzaman, A.; Lim, J.B.P.; Nash, D.; Roy, K. Cold-formed steel channel beams under end-two-flange loading condition: Design for edge-stiffened holes, unstiffened holes and plain webs. *Thin-Walled Struct.* **2020**, *147*, 106532. [CrossRef]
11. Uzzaman, A.; Lim, J.B.P.; Nash, D.; Roy, K. Web crippling behaviour of cold-formed steel channel sections with edge-stiffened and unstiffened circular holes under interior-two-flange loading condition. *Thin-Walled Struct.* **2020**, *154*, 106813. [CrossRef]
12. Janarthanan, B.; Mahendran, M.; Gunalan, S. Numerical modelling of web crippling failures in cold-formed steel unlipped channel sections. *J. Constr. Steel Res.* **2019**, *158*, 486–501. [CrossRef]
13. Janarthanan, B.; Sundararajah, L.; Mahendran, M.; Keerthan, P.; Gunalan, S. Web crippling behaviour and design of cold-formed steel sections. *Thin-Walled Struct.* **2019**, *140*, 387–403. [CrossRef]
14. Chen, Y.; Chen, X.; Wang, C. Experimental and finite element analysis research on cold-formed steel lipped channel beams under web crippling. *Thin-Walled Struct.* **2015**, *87*, 41–52. [CrossRef]
15. Gunalan, S.; Mahendran, M. Web crippling tests of cold-formed steel channels under two flange load cases. *J. Constr. Steel Res.* **2015**, *110*, 1–15. [CrossRef]
16. Winter, G.; Pian, R.H.J. *Crushing Strength of Thin Steel Webs, Engineering Experiment Station*; Cornell University: New York, NY, USA, 1946.
17. Young, B.; Hancock, G.J. Design of cold-formed channels subjected to web crippling. *J. Struct. Eng.* **2001**, *127*, 1137–1144. [CrossRef]
18. Macdonald, M.; Heiyantuduwa, M.A.; Kotelk, M.; Rhodes, J. Web crippling behaviour of thin-walled lipped channel beams. *Thin-Walled Struct.* **2011**, *49*, 682–690. [CrossRef]
19. Macdonald, M.; Heiyantuduwa, M.A. A design rule for web crippling of cold-formed steel lipped channel beams based on nonlinear FEA. *Thin-Walled Struct.* **2012**, *53*, 123–130. [CrossRef]
20. Keerthan, P.; Mahendran, M.; Steau, E. Experimental study of web crippling behaviour of hollow flange channel beams under two flange load cases. *Thin-Walled Struct.* **2014**, *85*, 207–219. [CrossRef]
21. Sundararajah, L.; Mahendran, M.; Keerthan, P. Experimental studies of lipped channel beams subject to web crippling under two-flange load cases. *J. Struct. Eng.* **2016**, *142*, 04016058. [CrossRef]
22. Sundararajah, L.; Mahendran, M.; Keerthan, P. New design rules for lipped channel beams subject to web crippling under two-flange load cases. *Thin-Walled Struct.* **2017**, *119*, 421–437. [CrossRef]

23. Alsanat, H.; Gunalan, S.; Guan, H.; Keerthan, P.; Bull, J. Experimental study of aluminium lipped channel sections subjected to web crippling under two flange load cases. *Thin-Walled Struct.* **2019**, *141*, 460–476. [CrossRef]
24. Alsanat, H.; Gunalan, S.; Poologanathan, K.; Guan, H. Web crippling capacities of fastened aluminium lipped channel sections subjected to one-flange loading conditions. *Structures* **2021**, *33*, 1754–1763. [CrossRef]
25. Alsanat, H.; Gunalan, S.; Keerthan, P.; Guan, H. Web crippling investigations of aluminium lipped channels under one-flange loading conditions. *Thin-Walled Struct.* **2021**, *166*, 108025. [CrossRef]
26. Alsanat, H.; Gunalan, S.; Keerthan, P.; Guan, H.; Tsavdaridis, K.D. Numerical investigation of web crippling in fastened aluminium lipped channels under two-flange loading conditions. *Structures* **2020**, *23*, 351–365. [CrossRef]
27. Alsanat, H.; Gunalan, S.; Keerthan, P.; Guan, H.; Tsavdaridis, K.D. Web crippling behaviour and design of aluminium lipped channel sections under two flange loading conditions. *Thin-Walled Struct.* **2019**, *144*, 106265. [CrossRef]
28. Zhou, F.; Young, B. Web crippling of aluminium alloy channel sections with flanges restrained. *Thin-Walled Struct.* **2020**, *148*, 106576. [CrossRef]
29. Chen, B.S.; Roy, K.; Fang, Z.Y.; Uzzaman, A.; Chi, Y.H.; Lim, J.B.P. Web crippling capacity of fastened cold-formed steel channels with edge-stiffened web holes, un-stiffened web holes and plain webs under two-flange loading. *Thin-Walled Struct.* **2021**, *163*, 107666. [CrossRef]
30. *AS/NZS 4600:2018*; Cold-Formed Steel Structures; Australia/New Zealand Standard (AS/NZS). Standards Australia: Sydney, Australia; Standards New Zealand: Wellington, New Zealand, 2018.
31. *AISI S100-16*; North American Specification for the Design of Cold-formed Steel Structural Members. American Iron and Steel Institute (AISI): Washington, DC, USA, 2016.
32. *AS/NZS 1664.1*; Aluminium Structures-Part 1: Limit State Design. Standards Australia (SA): Sydney, Australia, 1997.
33. Fang, Z.; Roy, K.; Ingham, J.M.; Lim, J.B.P. Assessment of end-two-flange web crippling strength of roll-formed aluminium alloy perforated channels by experimental testing, numerical simulation, and deep learning. *Eng. Struct.* **2022**, *268*, 114753. [CrossRef]
34. Ran, H.; Jian, L.; Ma, Y.; Sun, Y. Behavior of Stainless-Steel Hot-Rolled Channel Section Beam–Columns: Testing, Modeling, and Design. *J. Struct. Eng.* **2023**, *149*, 04022247. [CrossRef]
35. Sun, Y.; Fu, Z.; Song, Y.; Xia, J. Cross-Sectional Behavior of Aluminum Alloy Channel Section Stub Columns after Exposure to Fire. *J. Struct. Eng.* **2023**, *149*, 04023085. [CrossRef]
36. Sun, Y.; Liang, Y.; Zhao, O. Testing, numerical modelling and design of S690 high strength steel welded I-section stub columns. *J. Constr. Steel Res.* **2019**, *159*, 521–533. [CrossRef]
37. Sun, Y.; Zhao, O. Material response and local stability of high-chromium stainless steel welded I-sections. *Eng. Struct.* **2019**, *178*, 212–226. [CrossRef]
38. Ran, H.; Chen, Z.; Ma, Y.; OBrien, E.; Sun, Y. Experimental and numerical study of laser-welded stainless steel slender I-section beam-columns. *Eng. Struct.* **2023**, *286*, 116128. [CrossRef]
39. Feng, R.; Liu, J.; Chen, Z.; Roy, K.; Chen, B.; Lim, J.B.P. Numerical investigation and design rules for flexural capacities of H-section high-strength steel beams with and without web openings. *Eng. Struct.* **2020**, *225*, 111278. [CrossRef]
40. Fang, Z.; Roy, K.; Dai, Y.; Lim, J.B.P. Effect of web perforations on end-two-flange web crippling behaviour of roll-formed aluminium alloy unlipped channels through experimental test, numerical simulation and deep learning. *Thin-Walled Struct.* **2022**, *179*, 109489. [CrossRef]
41. Fang, Z.; Roy, K.; Ma, Q.; Uzzaman, A.; Lim, J.B.P. Application of deep learning method in web crippling strength prediction of cold-formed stainless steel channel sections under end-two-flange loading. *Structures* **2021**, *33*, 2903–2942. [CrossRef]
42. Dai, Y.; Roy, K.; Fang, Z.; Raftery, G.M.; Ghosh, K.; Lim, J.B.P. A critical review of cold-formed built-up members: Developments, challenges, and future directions. *J. Build. Eng.* **2023**, *76*, 107255. [CrossRef]
43. Feng, R.; Huang, Z.; Chen, Z.; Roy, K.; Chen, B.; Lim, J.B.P. Finite-element analysis and design of stainless-steel CHS-to-SHS hybrid tubular joints under axial compression. *Thin-Walled Struct.* **2020**, *151*, 106728. [CrossRef]
44. *ABAQUS Analysis User's Manual-Version 6.14-2*; ABAQUS Inc.: Palo Alto, CA, USA, 2018.
45. European Committee for Standardization (CEN). *Design of Aluminium Structures—Part 1.4: Cold-Formed Structural Sheeting*; Eurocode 9; European Committee for Standardization: Brussels, Belgium, 2007.